Two-dimensional lattice Boltzmann simulation of colloid migration in rough-walled narrow flow channels

H. Başağaoğlu*
Department of Geosciences, Oregon State University, Corvallis, Oregon 97331, USA

P. Meakin
Idaho National Laboratory, Center for Advanced Modeling and Simulation, P.O. Box 1625, MS 2211, Idaho Falls, Idaho 83415, USA

S. Succi
Instituto Applicazioni Calcolo, CNR-IAC Viale del Policlinico 137, 00161 Rome, Italy

G. R. Redden
Idaho National Laboratory, P.O. Box 1625, MS 2208, Idaho Falls, Idaho 83415, USA

T. R. Ginn
Department of Civil and Environmental Engineering, University of California, Davis, California 95616, USA
(Received 25 November 2007; revised manuscript received 18 February 2008; published 20 March 2008)

A lattice Boltzmann model was used to simulate the accelerated transport of dense inert particles in low Reynolds number flows in smooth- and rough-walled narrow channels. The simulations showed that, after an initial transient, an initially immobile particle migrated faster than the average fluid velocity. The sensitivity of the particle residence time to wall roughness increased with decreasing Reynolds numbers. The relationship between the exit position and residence time of a particle was sensitive to the release position, flow strength, and the wall roughness. A particle with a density 5% larger than the density of the fluid migrated to an equilibrium position between the centerline and the wall for the slowest flow rates in rough-walled channels, displaying the Segre-Silberberg effect that a rigid neutrally buoyant spherical particle exhibits in small Reynolds number flows. However, a particle that was 35% denser than the density of the fluid drifted to the centerline in the slowest flows due to the gravitational settling effect. The difference in the residence time of the less-dense and dense particles was most sensitive to the surface roughness at the smallest Reynolds number investigated.

DOI: 10.1103/PhysRevE.77.031405 PACS number(s): 83.80.Hj, 82.20.Wt

I. INTRODUCTION

There is a growing interest in the behavior of colloids in the subsurface because of their impact on the transport and distribution of anthropogenic contaminants and naturally occurring chemicals. Recently, the design of small particles for the optimal transport of therapeutic agents and their releases at desired sites in the human body has attracted attention in biomedical research and the pharmaceutical industry [1]. Similarly, the use of engineered particles for the efficient delivery of nutrients, oxygen sources, and other amendments to targeted contaminated sites in the subsurface for the purpose of stimulating bioremediation [2,3], mineral extraction or flow manipulations has also received considerable attention.

We report on lattice Boltzmann simulations of the trajectories of inert colloidal particles in pressure-driven low Reynolds number flows in smooth-walled and rough-walled channels. Several phenomena were investigated numerically including: (a) wall and inertial effects on particle trajectories, (b) particle size exclusion effects, (c) the effects of wall roughness on particle residence times in the channels and its implication for particle residence times on the continuum scale, (d) the effects of surface roughness on particle trajectories and its impact on the effective reaction rates and reaction times of reactive particles, and (e) the effects of particle density and initial release location on particle trajectories and residence times in channels with rough walls. These are key elements for the controlled delivery of particles in subsurface bioremediation and biomedical applications.

II. LATTICE BOLTZMANN (LB) COLLOIDAL TRANSPORT MODEL

In LB models, a fluid is represented by an ensemble of particles that stream along the bonds between the nodes of a regular lattice and undergo mass and momentum-conserving collisions at the nodes in each time step [4–6]. The microdynamics of the discretized LB equation with a single relaxation time [7] for single-phase flow is described by

$$f_i(\mathbf{r}+\mathbf{e}_i\Delta t, t+\Delta t) - f_i(\mathbf{r},t) = \frac{f_i^{\mathrm{eq}}(\mathbf{r},t) - f_i(\mathbf{r},t)}{\tau}, \qquad (1)$$

where $f_i(\mathbf{r},\mathbf{t})$ is the population density along the velocity vector $\mathbf{e}_i$ at position $\mathbf{r}$ and time t, f_i^{eq} is the equilibrium

*Current address: Center for Nuclear Waste Regulatory Analyses, Southwest Research Institute, San Antonio, TX 78238, USA.

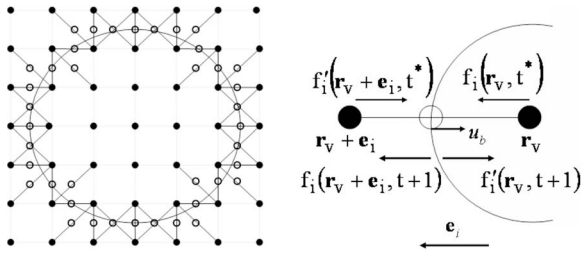

FIG. 1. Representation of a colloidal particle in the lattice Boltzmann model [9]. Open circles indicate the boundary nodes, filled circles inside the particle indicate intraparticle (virtual) fluid nodes, and filled circles outside the particle indicate bulk fluid nodes. The momentum transfer at the boundary node is shown in the right panel.

Maxwell-Boltzmann distribution function at the local flow velocity, τ is the relaxation parameter, which determines the kinematic viscosity of the fluid, $\mathbf{r}$ is the position of a lattice node, $\mathbf{r}=\mathbf{r}(x,y)$, where x and y are the Cartesian coordinates, and Δt is the time increment. A two-dimensional nine-velocity square lattice (D2Q9) model was used in this work. The discrete velocity vector basis for the D2Q9 model $\mathbf{e}_i$ consists of the null vector, four vectors of length unity directed toward the nearest neighbor nodes and four vectors of length $\sqrt{2}$ directed toward the next-nearest neighbor nodes. The discrete equilibrium Maxwell-Boltzmann distribution for the D2Q9 model is approximated by the low Mach number mass and momentum conserving expansion [8]

$$f_i^{\mathrm{eq}} = \omega_i \rho \left(1 + \frac{\mathbf{e}_i \cdot \mathbf{u}}{c_s^2} + \frac{(\mathbf{e}_i \cdot \mathbf{u})^2}{2c_s^4} - \frac{\mathbf{u} \cdot \mathbf{u}}{2c_s^2} \right), \tag{2}$$

where ω_i is the weight coefficient for the ith vector (4/9 for the null vector, 1/9 for the vectors directed along the $\pm x$ and $\pm y$ axes, and 1/36 for the diagonal vectors), c_s is the sound velocity, and $\mathbf{u}$ is the macroscopic fluid velocity at the lattice node. The local macroscopic density and velocity at a lattice site can be computed from the distribution functions at that site from $\rho=\Sigma_i f_i$ and $\rho\mathbf{u}=\Sigma_i f_i \mathbf{e}_i$.

A LB model for colloidal transport was first formulated in Ref. [9] based on the premises that (a) the fluid occupies the regions inside and outside the particles, (b) the momentum exchange between the suspended particle and the fluid occurs at boundary nodes located half-way between the fluid nodes inside and outside the particle nearest to the particle surface, and (c) fluid motion obeys the nearly incompressible Navier-Stokes equation. The assumption in (a) was later relaxed by introducing virtual intraparticle fluid nodes [10] that do not contribute to the momentum transfer at the boundary nodes. In this case, the hydrodynamic force at a boundary node $\mathbf{r}_b$ on the particle surface located between an intraparticle (virtual) fluid node at $\mathbf{r}=\mathbf{r}_v$ and an extra-particle fluid node at $\mathbf{r}=\mathbf{r}_v+\mathbf{e}_i\Delta t$ (Fig. 1) is given by

$$\mathbf{F}_{\mathbf{r}_b} = -2 \left[f_i'(\mathbf{r}_v + \mathbf{e}_i \Delta t, t^*) + \frac{\rho \omega_i}{c_s^2} (\mathbf{u}_{\mathbf{r}_b} \cdot \mathbf{e}_i) \right] \mathbf{e}_i, \tag{3}$$

where t^* indicates the post-collision time, f_i' is the population density in the $-\mathbf{e}_i$ direction and $\mathbf{u}_{\mathbf{r}_b}$ is the velocity at the boundary node. Additional small force (and torque) impulses are transferred to the particle as the lattice nodes are covered or uncovered due to the particle motion. They are proportional to the difference between the local velocity at the (un)covered node and the particle velocity [10]. These forces are given by

$$\mathbf{F}_{\mathbf{r}_b^{c,u}} = \pm \rho(\mathbf{u}_{\mathbf{r}_b} - \mathbf{U}), \quad \mathbf{T}_{\mathbf{r}_b^{c,u}} = (\mathbf{r}_b^{c,u} - \mathbf{r}_c) \times \mathbf{F}_{\mathbf{r}_b^{c,u}}. \tag{4}$$

The sign in Eq. (4) is positive when the lattice node is covered by the particle, and negative when it is uncovered. The total hydrodynamic force applied to the particle $\mathbf{F}_T$ is given by $\Sigma_{\mathbf{r}_b}\mathbf{F}_{\mathbf{r}_b}+\Sigma_{\mathbf{r}_b^{c,u}}\mathbf{F}_{\mathbf{r}_b}^{c,u}$. The total torque $\mathbf{T}_T$ exerted on the particle by the surrounding fluid is given by $\mathbf{T}_T=\Sigma_{\mathbf{r}_b}(\mathbf{r}_b-\mathbf{r}_c) \times \mathbf{F}_{\mathbf{r}_b}$ where $(\mathbf{r}_b-\mathbf{r}_c)$ is the distance from the boundary node at position $\mathbf{r}_b$ to the particle center at $\mathbf{r}_c$. The translational velocity $\mathbf{U}$ and the angular velocity of the particle $\mathbf{\Omega}$ can be computed from Newton's second law using first order accurate Euler integration

$$\mathbf{U}(t+1) \equiv \mathbf{U}(t) + \frac{\Delta t}{m_p} \mathbf{F}_T(t) + \frac{\Delta t}{\rho_p} (\rho_p - \rho)\mathbf{g}, \tag{5}$$

$$\mathbf{\Omega}(t+1) \equiv \mathbf{\Omega}(t) + \frac{\Delta t}{I_m} \mathbf{T}_T(t), \tag{6}$$

where ρ_p is the particle density, m_p is the particle mass, and I_p is the moment of inertia of a circular particle ($I=2mR^2/5$). In this work, the time required for streaming between a node and its neighbors was used as the unit of time ($\Delta t=1$). The local velocity of a particle at the boundary nodes is given by $\mathbf{u}_b=\mathbf{U}+\mathbf{\Omega}\times(\mathbf{r}_b-\mathbf{r}_c)$. The new position of the center of the colloidal particle can be computed from $\mathbf{r}_c(t+1)=\mathbf{r}_c(t)+\mathbf{U}(t)\Delta t$, and the population densities at $\mathbf{r}_v$ and $\mathbf{r}_v+\mathbf{e}_i\Delta t$ can be computed as

$$f_i'(\mathbf{r}_v, t+1) = f_i(\mathbf{r}_v, t^*) - \frac{2\rho\omega_i}{c_s^2}(\mathbf{u}_b \cdot \mathbf{e}_i), \tag{7}$$

$$f_i(\mathbf{r}_v + \mathbf{e}_i\Delta t, t+1) = f_i'(\mathbf{r}_v + \mathbf{e}_i\Delta t, t^*) + \frac{2\rho\omega_i}{c_s^2}(\mathbf{u}_b \cdot \mathbf{e}_i). \tag{8}$$

III. MAIN FEATURES OF THE SIMULATIONS

(1) Flow was assumed to be driven by a uniform gravitational acceleration acting along the axes of the two-dimensional channels. Gravity $\mathbf{g}$ was introduced in the form of an altered flow velocity field [11], in which the fluid velocity in Eqs. (1) and (2) was computed from $\rho\mathbf{u}=\Sigma_i f_i \mathbf{e}_i + \tau\rho\mathbf{g}$.

(2) A single inert particle was used in the simulations to eliminate the effects of particle-particle hydrodynamic interactions on the particle trajectories. Unless otherwise stated, the particle was assumed to be 5% denser than the fluid and it was released into the flow domain after quasi-steady-flow was established.

(3) No-slip boundary conditions were imposed at the channel walls parallel to the main flow direction. Periodic

TABLE I. Flow parameters for seven different flow conditions C1–C7.

Parameters	C1	C2	C3	C4	C5	C6	C7
Re	9.29	21.25	25.62	26.79	27.63	28.55	29.63
ν	0.107597	0.116667	0.111667	0.108667	0.106667	0.104667	0.100667
g	0.000065	0.000168	0.000190	0.000190	0.000190	0.000190	0.000190

boundary conditions were used along the in-flow and exit ends of the smooth-walled and rough-walled flow domains. The length of the flow channel was set to 75 times longer than the average hydrodynamic channel width.

(4) For rough-walled simulations, the channel walls were roughened by adding uncorrelated random displacements ϵ uniformly distributed over the range $(-\epsilon^* \leq \epsilon \leq \epsilon^*)$ (ϵ^* defines the upper and lower bounds of the perturbation) perpendicular to the wall. Perturbations with $|\epsilon| \leq 0.10w$ were used to generate a flow channel with irregular surfaces (for $|\epsilon| > 0.10w$ the upper portion of the particle and the upper rough-walled boundary would overlap). Textures with $|\epsilon| \leq 0.10w$ were imposed on each side of the channel. This increased the average flow channel aperture by 0.1%, and changed the local flow channel aperture by up to $0.2w$.

IV. SMOOTH-WALLED FLOW CHANNEL

Trajectories of an inert particle were simulated in a smooth-walled rectangular flow channel under low Reynolds number flow conditions. The center of a stationary particle was initially placed 20% of the channel width w ($0.2w$) from the centerline. The Reynolds number (Re) was defined as $\mathrm{Re}=2Ru_{\mathrm{avg}}/\nu$, where R is the particle radius [which was set to 7.5 lattice unit ($0.19w$)], u_{avg} is the average flow velocity before the particle was released, and ν is the kinematic viscosity $\nu=c_s^2(\tau-\Delta t/2)$. Particle migration in seven different Reynolds number flows (C1–C7) was studied (Table I).

For all flow rates investigated, the particle migrated across streamlines, and this is consistent with earlier investigations [12,13]. The transitions from (i) monotonic migration of the particle to a steady position in the channel at low Re (C1 and C2) to (ii) a nearly steady equilibrium with transient overshoot at higher Re (C3, C4, and C5), and then to (iii) periodic or oscillatory trajectories (C6 and C7) as Re is further increased agree well with the behaviors found in Ref. [13]. The results in Fig. 2 suggest that the inertial effects are largely responsible for transient overshoots in particle trajectories in smooth-walled channels.

When the particle is off the centerline, it rotates until it approaches a steady equilibrium position near the centerline [Fig. 2(d)] due to asymmetric hydrodynamic forces on the opposite sides of the particle. This has been reported as a typical behavior for non-neutrally buoyant dense particles in smooth-walled channels [13,14]. As the particle moves closer to the lower channel wall, the pressure gradient between the particle and the lower channel wall becomes steeper than the pressure gradient between the particle and the upper channel wall in the direction of the channel (not shown here). This causes the particle to rotate in the counter clockwise direction, and it appears to roll along the nearest channel wall as it drifts from the nearest wall to the centerline [Fig. 2(d)]. For C1–C3, the angular velocity approached zero at or before the particle approached the exit-end of the flow channel.

As the Reynolds number decreased, the particle residence time increased (the travel time of the particle was 2.5 times longer for C1 than for C7). To analyze the size-exclusion effect, the particle velocity was compared with the average fluid velocity $u_{\mathrm{avg}}(x_c)$:

$$u_{\mathrm{avg}}(x_c) = \frac{1}{N(x_c)} \sum_{j=l(x_c)}^{r(x_c)} u(j), \tag{9}$$

where $l(x_c)$ and $r(x_c)$ are the position of boundary nodes on opposite sides of the channel walls aligned orthogonal to the main flow direction at $x=x_c$. $N(x_c)$ is the number of fluid nodes (indexed by j) between $l(x_c)$ and $r(x_c)$ and $u(j) = \sqrt{u_x(j)^2+u_y(j)^2}$. The temporal variations of the difference between the translational velocity of a particle and the average local velocity of the fluid $U|_{x=x_c} - u_{\mathrm{avg}}(x_c)|_t$ as a function of u_{avg} is shown in Fig. 3. Figure 3(b) shows that as the Reynolds number increased, the average velocity of the fluid increased while the difference between the average particle velocity and the average fluid velocity displayed a larger variation with respect to changes in the average fluid velocity for these fast flows. In these simulations the particle was repelled from low velocity zones near the flow channel boundaries and stayed at or near the high velocity zone while experiencing higher convective velocities than the average solute velocity in a narrow channel.

Laboratory column and micromodel experiments have demonstrated that colloidal particles can migrate faster than the average carrier fluid velocity in porous [15] and fractured [16] media. Size exclusion was briefly analyzed in terms of Taylor-Aris transport of a Brownian colloid in Poiseulle flow in Ref. [17], where it was shown that the effective velocity of the colloid was larger and the dispersivity was smaller than that of a solute tracer. Both within-pore streamline restriction (size exclusion) and detours (pore exclusion) in laboratory micromodel experiments were observed in Ref. [18]. In this work, the definition of size exclusion effect complies with the observation in Fig. 3.

V. FLOW CHANNELS WITH ROUGH SURFACES

The surface asperities were introduced as described in Sec. II. Trajectories of a particle across smooth-walled ($\epsilon^*=0.0$) and rough-walled ($\epsilon^*=0.055w$ and $0.10w$) flow channels are shown in Fig. 4. Due to locally perturbed ve-

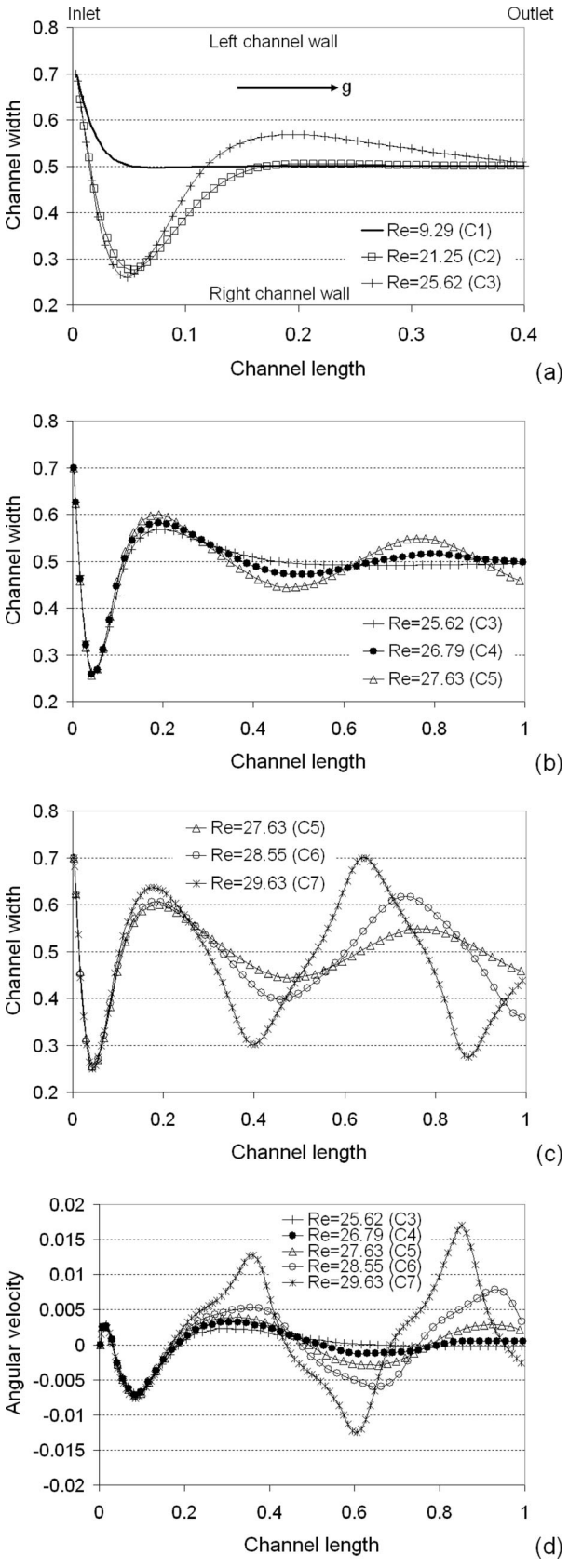

FIG. 2. Trajectories of a particle under different flow conditions C1–C3 (a), C3–C5 (b), and C5–C7 (c). The angular velocity of a particle under different flow conditions are shown in (d).

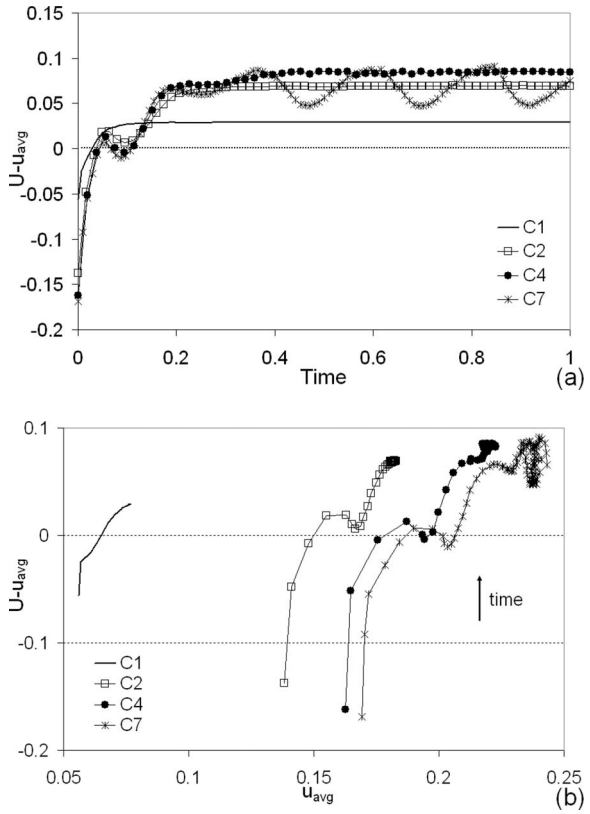

FIG. 3. The difference between particle velocity and the averaged flow velocity of the fluid $U|_{x=x_c} - u_{\mathrm{avg}}(x_c)|_t$ in time (a) and with respect to u_{avg} (b).

locity and pressure fields near the channel walls imposed by the surface roughness, the particle constantly rotated throughout its flow path (with nonzero angular velocities), unlike the behavior in the smooth-walled channel (Fig. 5).

For C4 and C7, the oscillations in the particle trajectory diminished as the surface roughness became more pronounced, suggesting that the inertial effects on the particle trajectory [19] was weakened by nonuniform flows imposed by channel wall irregularities, and the particle drifted to and stayed near the centerline of the channel (for $\epsilon^*=0.10w$, the Reynolds numbers decreased from 9.29, 26.79, and 29.63 to 6.29, 18.10, and 19.85, due to the surface roughness, for C1, C4, and C7, respectively). Near the exit end of the rough-walled flow channel (with $\epsilon^*=0.10w$), the particle stayed closer to the left channel wall (11% off the centerline) in C1 (similar to the Segre-Silberberg effect [20,21] that a rigid spherical and neutrally buoyant particle exhibits in slow flows [22]), whereas it remained closer to the centerline (within 2%) in C4 and C7, and this was different from their trajectories in the smooth-walled flow channel (the Segre-Silberberg effect is the concentration of neutrally buoyant particles suspended in a fluid flowing a channel with a circular cross section onto a narrow annular region separated from both the wall and the axis).

The residence time of the particle in the flow channel increased as the magnitude of the wall roughness increased [Fig. 4(d)]. As the magnitude of the surface irregularity was increased to $\epsilon^*=0.10w$, the residence time of the particle

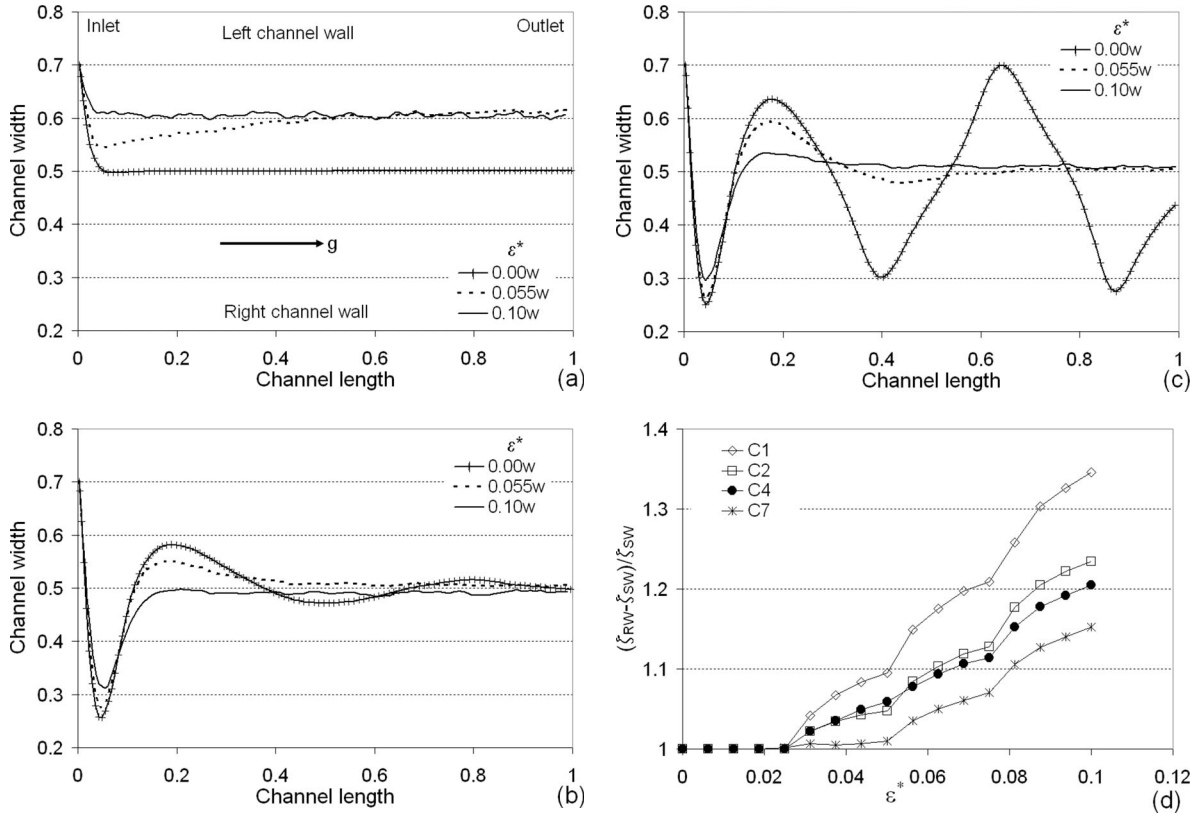

FIG. 4. Trajectories of a particle under different flow conditions in a rough-walled rectangular flow channel for C1 (a), C4 (b), and C7 (c). Part (d) shows the percent increases in the residence time ζ of the particle in the rough-walled (RW) channels compared to the residence time in the smooth-walled (SW) channel as a function of the roughness amplitude ϵ^*.

increased by a factor of 1.35 for C1 and 1.15 for the C7, because the particle experienced a wider distribution of convective velocities in the nonuniform flow field in the rough-walled channel than in the uniform flow field in the smooth-walled channel. Hence, the residence time of the particle was more sensitive to the wall roughness in slow flow fields than in fast flow fields. Although the particles did not interact directly with the walls in these simulations, longer residence times caused by surface roughness for interacting particles would provide more opportunity for physical and chemical interactions between the particle and the channel walls. This phenomenon has been observed in the particle tracking simulations reported in Ref. [23], where an increase in the fracture aperture variability resulted in an increase in the particle residence time. This increases in residence time could significantly affect targeted delivery of synthetic particles in bioremediation and biomedical applications.

The difference between the particle velocity and the averaged flow velocity exhibited larger variations in rough-walled channels than in the smooth-walled channel. In order to quantify the variations in the velocity differences, the velocity difference time series [e.g., Fig. 6(a)] were converted into detrended series by removing the time-averaged velocity difference (trend) [24]. The variance of the detrended velocity differences in the rough-walled channel with $\epsilon^*=0.10w$ were 47, 24, 17, and 15 times higher for C1, C2, C4, and C7, respectively, relative to the smooth-walled channel [Fig. 6(b)].

For all flow conditions considered herein, the increases in particle residence time in a rough-walled channel showed strong correlations with the variance of the differences between the particle velocity and local average velocity, which increased with increasing wall roughness (Fig. 7). This explains why particles in rough-walled channels have longer residence times than the same particles in smooth-walled channels, as observed in earlier continuum-scale analyses. The smaller hydrodynamic width of the rough-walled channels and strong hydrodynamic screening effects also contribute to the longer residence time.

When the particle is used as a delivery vehicle consisting of amendments encapsulated in a soluble layer (e.g., drug delivery), the average fluid velocity, relative to the particle velocity, in the immediate vicinity of the particle has an important impact on the dissolution rate. In a pressure-driven fluid flow, the average fluid velocity around the particle edge was smaller in a rough-walled flow channel than in a smooth-walled channel (Fig. 8). Although velocity-dependent dissolution kinetics could be enhanced in smooth-walled channels due to higher velocities near the particle edge, the particle residence time would be longer in rough-walled channels [Fig. 4(d)], which would increase the reaction time of the particle. Hence, if reactive agents are coated with a soluble material, the particle reaction rate would be increased by the relatively higher fluid velocity at the particle edge in smooth-walled channels. However, in rough-walled channels, the reaction time would be increased by the relatively longer residence time of the particle.

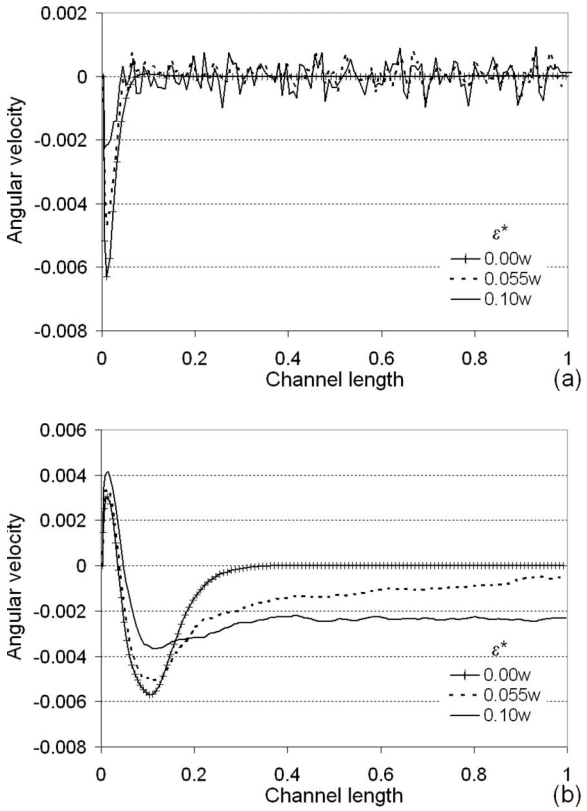

FIG. 5. Variation in the angular velocity with position along the channel for a particle that was released from a point $0.2w$ off the centerline in rough-walled and smooth-walled channels under flow conditions C1 (a) and C2 (b).

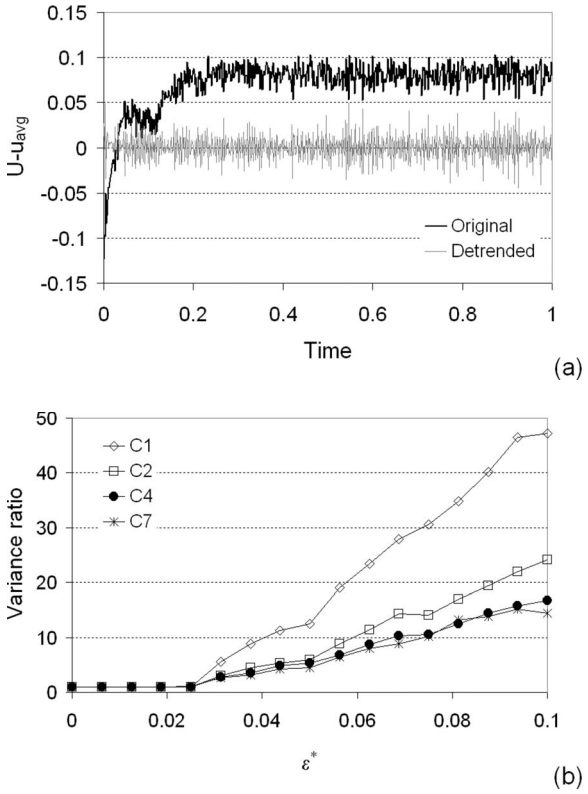

FIG. 6. The difference between the particle velocity and the averaged fluid flow velocity $U-u_{\mathrm{avg}}$ after a dense particle was released into a flow channel is shown for C4 for $\epsilon^*=0.10$ (a). The normalized (with respect to results from smooth-walled) variance of the fluctuations in $U-u_{\mathrm{avg}}$ is shown for different surface roughness magnitudes, as a fraction of the channel width w (b).

VI. EFFECTS OF THE PARTICLE RELEASE LOCATION ON TRANSPORT

A particle was released into rough-walled flow channels from different points (less than $0.2w$ from the centerline in both direction at $x=0.08$), and the effects of the release location on the position of the particle near the exit end and the changes in the residence time of the particle with respect to the reference scenario (in which a particle was released at $x=0.08$, $y=0.3$ in each case) are shown in Fig. 9. The exiting position of the particle exhibited the widest distribution for the slowest flows for both $\epsilon^*=0.055w$ and $\epsilon^*=0.10w$. The relation between the release and exiting positions of the particle could be represented by sinusoidal curves for C1, C4, and C7, but an inverse sigmoid curve for C2 with $\epsilon^*=0.055w$. An increase in the magnitude of the wall roughness (to $\epsilon^*=0.10w$) transformed the relation between the release and exiting positions of the particle into a sigmoid curve for C1. For C2 and C4, the relation, however, could be represented by inverse sigmoid curves. The range of particle exit positions became narrower as the flow strength increased, suggesting that the boundary effects decreased as the residence time of the particle decreased. A wider range of exit positions, in addition to longer travel times [Fig. 4(d)] in channels with more pronounced wall roughness would, in practice, promote physical and chemical interactions between the particle and channel walls.

The results indicate that if the particle is required to arrive closer to the right channel wall near the exit-end of the rough-walled channel (with $\epsilon^*=0.10w$) for C1, the particle should be released from a point between the centerline and right channel wall. However, for C2, in the same channel and for a similar targeted location, the particle should be released from a point between the centerline and the left channel wall. When the same size particle was released from $y=0.3$, the exiting position of the particle in C1 and C2 was $2R$ ($\sim 0.4w$). For C4 and C7, however, the exiting position of the particle was relatively less sensitive to the release location in a rough-walled channel. When the particle was released from the centerline of the channel, it constantly stayed closer to the centerline while experiencing the shortest travel time under all the flow conditions investigated. In most practical applications, a large number of particles is released, and it would be impractical to control how each particle was released into the flow domain. The model, however, has the capability to simulate the effect of the release location on the exit position and travel time of a particle.

The distribution of travel times was widest for C1 and C2 and narrowest for C4 and C7 in the rough-walled channel with $\epsilon^*=0.10w$. For the flow channel with the small wall roughness ($\epsilon^*=0.05w$), the distribution was widest for C1 but still relatively wide for C7. A drastic change in the distribution of travel times with respect to the release location

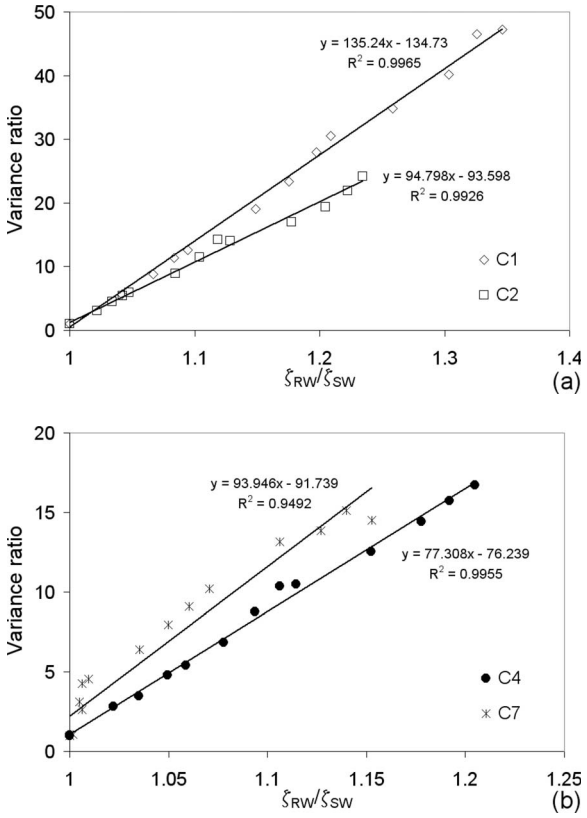

FIG. 7. Correlations between the normalized (with respect to results from smooth-walled) variance of the fluctuations in $U-u_{\mathrm{avg}}$ and the increase in the residence time ζ of the particle in a flow channel (with respect to its residence time in a smooth-walled channel) with different channel-wall roughnesses for C1 and C2 (a) and C4 and C7 (b). R^2 is the correlation coefficient.

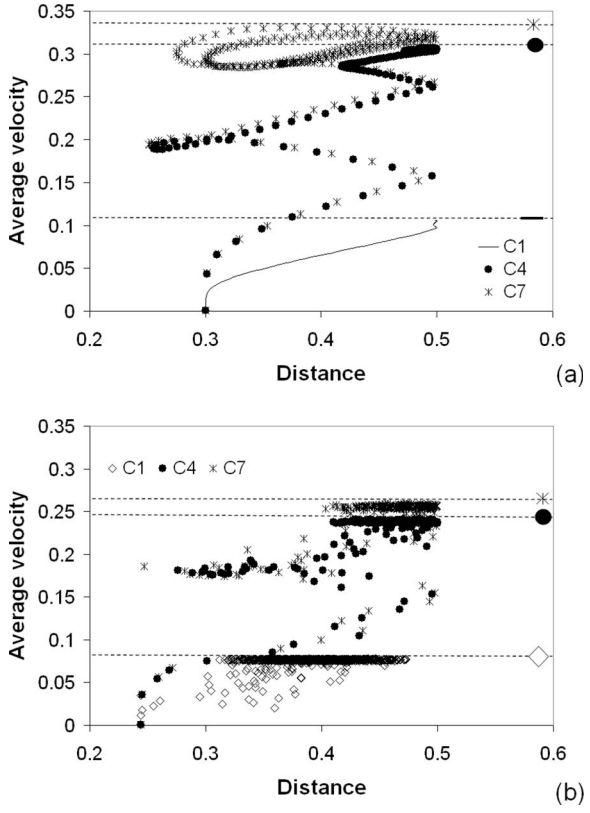

FIG. 8. Average fluid velocity in the immediate vicinity of the particle vs distance between the particle center and the closest channel wall in a smooth-walled channel (a) and a rough-walled flow channel with $\epsilon^*=0.10w$ (b). Dashed lines mark the maximum average fluid velocity in the immediate vicinity of the particle.

was observed for C1 when the magnitude of the wall roughness was doubled, because the residence time of the particle was found to be most sensitive to the magnitude of the wall roughness for the low Reynolds number flows [Fig. 4(d)]. Figure 9 also shows that if a longer reaction time with the surrounding fluid in the rough-walled channel is desired, the particle should be released from a point $0.2w$ from the centerline (on either side of the channel) for high Reynolds number flows, but preferably from a point $0.2w$ from the centerline toward the left wall in C1. Briefly, the residence time and exit position of the initially stationary particle are sensitive to the release point of the particle, the flow strength, and the magnitude of wall roughness in the channel.

VII. EFFECTS OF THE PARTICLE DENSITY ON THE TRANSPORT

Particles that were 5 and 35 % ($\rho_p=1.05$ and $\rho_p=1.35$) denser than the fluid density were released into a flow domain at a point $0.2w$ off the centerline toward the channel wall. For both $\epsilon^*=0.05w$ and $\epsilon^*=0.10w$, the less-dense ($\rho_p=1.05$) particle followed a path between the centerline and the left wall, exhibiting the Segre-Silberberg effect ([20,21] that a rigid and neutrally buoyant spherical particle displays in slow flow fields [22]). The dense ($\rho_p=1.35$) particle, however, drifted toward the centerline due to larger gravitational settling effects. For $\epsilon^*=0.055w$, the dense particle trajectory in high Reynolds number flows displayed larger overshoots than the less-dense particle due to relatively higher inertial effects while the particles settle under gravity, but eventually drifted to the centerline. For $\epsilon^*=0.10w$, both the less-dense and dense particles quickly drifted to the centerline in higher Reynolds number flows [Figs. 10(a)–10(c)].

The position of the dense particle relative to the less-dense particle at any particular time is given in Figs. 10(b)–10(d). For both $\epsilon^*=0.055w$ and $\epsilon^*=0.10w$, the dense particle reached the exit of the flow domain ahead of the less-dense particle by 11% of the distance traveled by the less-dense particle in the slowest flow. However, in the faster flows (C4 and C7), the dense particle was ahead of the less-dense particle by only 4%. The relative distance between the dense and less-dense particle became smaller at higher flow rates. The simulation results showed that in the slowest flow, the less-dense particle moved closer to the channel walls and had a longer residence time in the flow channel than the dense particle. Hence, channel-wall interactions and reaction times are expected to be larger for less-dense particles than dense particles in slow flow fields in rough-walled channels.

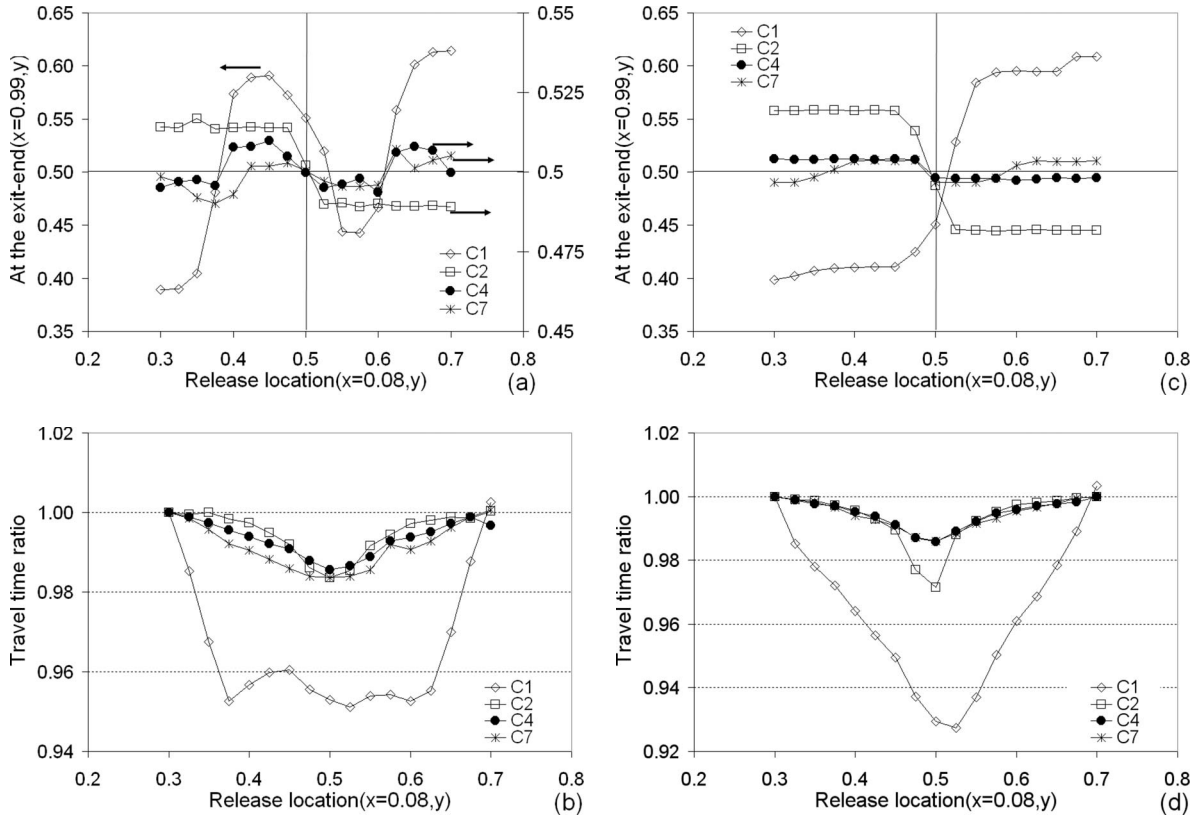

FIG. 9. The exiting position of a particle that was released at different points $x=0.08$, $y=0.3-0.7$ ($y=0$ is the left channel wall and $y=0.5$ is the centerline) for $\epsilon^*=0.055w$ (a) and $\epsilon^*=0.10w$ (c). The ratio of the residence time of the particle released at different points to the travel time of the particle released at $x=0.08$, $y=0.3$ for $\epsilon^*=0.055w$ (b) and $\epsilon^*=0.10w$ (d).

VIII. CONCLUSIONS

A LB model was used to simulate trajectories of individual inert particles through narrow smooth-walled and rough-walled channels under relatively low Reynolds number flow conditions. The LB simulations were performed using a two-dimensional model, and they can provide only a qualitative indication of the behavior of three-dimensional experimental systems. The simulations revealed the impact of surface roughness on the residence time of inert particles in narrow fracture channels, although such effects have often been neglected in continuum-scale colloidal transport models.

For smooth-walled channels, the LB model captured the wall effects on the lateral migration of the particle and the inertial effects on particle trajectories when the particle release point was off the centerline. After a transition period, an initially immobile particle consistently moved faster than the average velocity of the fluid for all flow rates in both smooth- and rough-walled narrow channels. As the Reynolds number gradually increased, the particle trajectories displayed transitions from (i) monotonic migration to a steady position at the centerline, to (ii) a nearly steady equilibrium with transient overshoot, and (iii) to oscillatory trajectories. At higher Reynolds number flows, the frequency and amplitude of the oscillation becomes larger as the distance from the release point increased.

The colloid residence time increased with increasing fracture aperture variability in continuum-scale numerical simulations [23], and the LB simulations indicate that a longer particle residence time in rough-walled channels was accompanied by higher statistical variance of the difference between the pore-scale particle velocity and the average flow velocity in channels with more pronounced surface asperities. The residence time of the particle was more sensitive to the wall roughness in slow flow fields than in fast flow fields. Relatively higher fluid velocities at the edge of a particle in smooth-walled channels and relatively longer residence times in rough-walled channels would determine the reaction time of a particle, if the particle was reactive.

The exit positions and travel times of particles were sensitive to the release location, flow strength, and the magnitude of surface asperities. The relation between the particle release and exit positions could be represented by sigmoid curves at the lowest flow strength, inverse sigmoid curves at relatively higher flow strengths, and sinusoidal curves at high flows in channels with large asperities. The sensitivity of the exit position to the particle release point decreased with increasing flow strength. The travel time of the particle displayed a wider distribution for the slowest flow and a narrower distribution for the higher flows in the roughest-walled channel. The less-dense particle migrated to an equilibrium position between the centerline and the wall in the slowest flow in a rough-walled channel, displaying the Segre-Silberberg effect [20,21] that a rigid spherical and neutrally

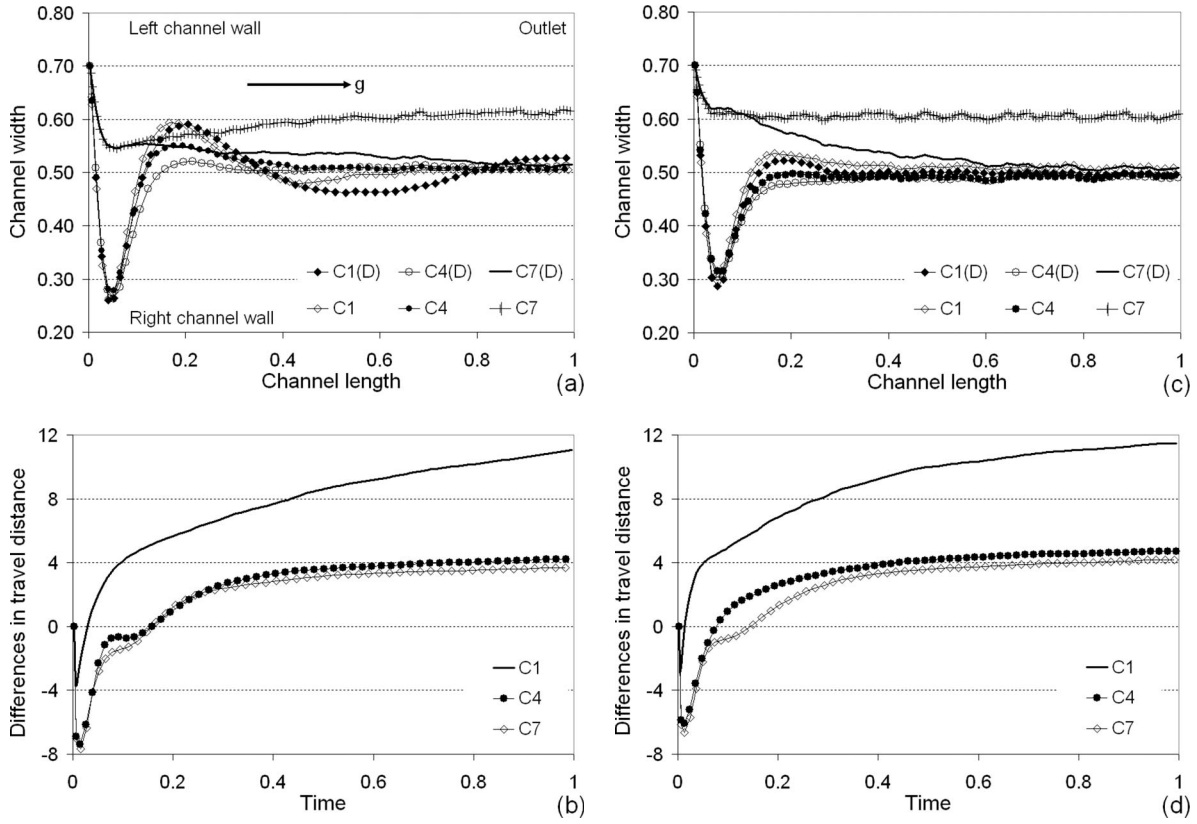

FIG. 10. Position of dense (d), and less-dense particles in a rough-walled flow channel with $\epsilon^*=0.055w$ (a) and $\epsilon^*=0.10w$ (c). The differences in the travel distance for the dense and less-dense particle in reference to the distance traveled by the less-dense particle as a function of time for $\epsilon^*=0.055w$ (b) and $\epsilon^*=0.10w$ (d).

buoyant particle exhibits in low Reynolds number flows [22]. The dense particle, however, drifted to the centerline due to the larger gravitational settling effect. The less-dense and dense particles drifted to the centerline at high flows although flow trajectories displayed some variations. Hence, the interplay between the gravitational settling and the inertial effects influenced by the wall roughness determined the quasi-equilibrium position of the particle. The travel time differences of the less-dense and dense particle was most sensitive to the surface roughness for the slower flows.

ACKNOWLEDGMENTS

This work was supported by the U.S. Department of Energy Environmental Management Science Program under Contract No. DE-AC07-05ID14517 at the Idaho National Laboratory.

[1] K. Kostarelos, Adv. Colloid Interface Sci. **106**, 147 (2003).
[2] W. Tungittiplakorn, C. Cohen, and L. W. Lion, Environ. Sci. Technol. **39**, 1354 (2005).
[3] D. W. Elliott and W.-X. Zhang, Environ. Sci. Technol. **35**, 4922 (2001).
[4] R. Benzi, S. Succi, and M. Vergassola, Phys. Rep. **222**, 145 (1992).
[5] D. A. Wolf-Gadrow, *A Lattice Gas Cellular Automata and Lattice Boltzmann Model* (Springer-Verlag, Berlin, 2000).
[6] S. Succi, *The Lattice-Boltzmann Equation* (Oxford University Press, New York, 2001).
[7] P. L. Bhatnagar, E. P. Gross, and M. A. Krook, Phys. Rev. **94**, 511 (1954).
[8] Y. H. Qian, D. D'Humieres, and P. Lallemand, Europhys. Lett. **17**, 479 (1992).
[9] A. J. C. Ladd, J. Fluid Mech. **271**, 285 (1994).
[10] E.-J. Ding and C. K. Aidun, J. Stat. Phys. **112**, 685 (2003).
[11] J. M. Buick and C. A. Greated, Phys. Rev. E **61**, 5307 (2000).
[12] C. K. Aidun, Y. Lu, and E.-J. Ding, J. Fluid Mech. **373**, 287 (1998).
[13] J. Feng, H. Hu, and D. D. Joseph, J. Fluid Mech. **261**, 95 (1994).
[14] D. Qi, L. Luo, R. Aravamuthan, and W. Strieder, J. Stat. Phys. **107**, 101 (2002).
[15] S. Sirivithayapakorn and A. Keller, Water Resour. Res. **39**, WR001223 (2003).

[16] R. B. Knapp, M. L. Chiarappa, and W. B. Durham, Water Resour. Res. **36**, 3139 (2000).
[17] H. Brenner and D. A. Edwards, *Macrotransport Process* (Butterworth-Heinemann, Boston, MA, 1993).
[18] M. Auset and A. A. Keller, Water Resour. Res. **40**, W03503 (2004).
[19] J. Happel and H. Brenner, *Low Reynolds Number Hydrodynamics* (Prentice-Hall, Upper Saddle River, NJ, 1965).
[20] G. Segre and A. Silberberg, Nature (London) **189**, 209 (1961).
[21] G. Segre and A. Silberberg, J. Fluid Mech. **14**, 115 (1962).
[22] B. P. Ho and L. G. Leal, J. Fluid Mech. **65**, 365 (1974).
[23] S. James and C. Chrysikopoulos, Water Resour. Res. **34**, 1901 (2000).
[24] R. H. Shumway and D. S. Stoffer, *Time Series Analysis and Its Applications* (Springer, New York, 2000).